ELSEVIER

Polymer 44 (2003) 1705–1710

polymer

www.elsevier.com/locate/polymer

Alignment and orientational proliferation of HEX cylinders in a polystyrene-*block*-polyisoprene-*block*-polystyrene copolymer in the presence of clay

Jae Young Lee, Min Soo Park, Hoi Chang Yang, Kilwon Cho, Jin Kon Kim*

Department of Chemical Engineering and Polymer Research Institute, Electronic and Computer Engineering Divisions, Pohang University of Science and Technology, Kyungbuk 790-784, South Korea

Received 8 May 2002; received in revised form 25 October 2002; accepted 27 November 2002

Abstract

We investigated the effect of an anisotropic silicate layer on the alignment and orientational proliferation of hexagonally packed cylinder microdomains of a block copolymer in the presence of a clay by using synchrotron small angle X-ray scattering (SAXS), rheology, and transmission electron microscopy (TEM). The block copolymer employed in this study was polystyrene-*block*-polyisoprene-*block*-polystyrene copolymer (SIS). The degree of intercalation of the clay in the presence of SIS was examined by wide angle X-ray diffraction (WAXD).

Almost all of the HEX cylinders in neat SIS are aligned toward the flow direction after large amplitude oscillatory shearing is applied to the specimens. However, some tactoids in nanocomposites are not aligned, although most tactoids are also aligned to the flow direction. Due to HEX cylinders near tactoids, which are not aligned to the flow direction, the orientational factor of HEX cylinders in SIS/clay nanocomposites is smaller than that of neat SIS. However, once HEX cylinders in SIS/clay nanocomposites are degenerated after experiencing body-centered cubic microdomains, the decrease in the orientational factor from original aligned HEX is smaller compared with neat SIS.

Keywords: Nanocomposites; Block copolymer; Orientation

1. Introduction

Polymer/clay nanocomposites have been studied extensively due to their excellent thermal and mechanical properties compared with inorganic filler-based polymer composites [1]. Several polymers, for instance, polyamide (Nylon 6) [2], polystyrene (PS) [3–7], poly(methyl methacrylate) [8], poly(propylene) [9], poly(ethylene oxide) [10], epoxy [11], and polymer liquid crystal [12], have been employed. Krishnamoorti and co-workers [13] studied the block copolymer-based nanocomposites. For polystyrene-*block*-polyisoprene (SI) copolymer based nanocomposites, the increase in the clay galley layer (or intercalation degree) was larger than that in PS-based nanocomposite. They explained that even though the clay gallery layer does not increase for polyisoprene (PI)/clay nanocomposites, PI chains could penetrate between the galley together with PS chains due to the connection to the PS chains as well as short PS block chains. These portions of PI chains result in further intercalation compared with PS chains themselves. However, the gallery layer does not change with the amount of block copolymer.

Very recently, they [14,15] also investigated the order-to-disorder transition (ODT) and the order-to-order transition (OOT) between hexagonally packed cylinder microdomains (HEX) and body-centered cubic microdomains (BCC) using a polystyrene-*block*-poly(ethylene-*co*-butylene)-*block*-polystyrene (SEBS). Interestingly, when the specimens were jumped from a disordered state to BCC, the ordering kinetics of PS spheres in the clay/SEBS nanocomposites were much faster than that of SEBS itself due to enhanced nucleation by the clay. But, when the specimens were jumped from a disordered state to HEX, the ordering kinetics of SEBS was not changed with the presence of the clay. The reason was that the length of PS

* Corresponding author. Tel.: +82-54-279-2276; fax: +82-54-279-8298.
E-mail address: jkkim@postech.ac.kr (J.K. Kim).

0032-3861/03/$ - see front matter © 2003 Elsevier Science Ltd. All rights reserved.
PII: S0032-3861(02)00912-6

cylinder is larger than the size of the clay; thus the clay does not play a role as a template for enhanced nucleation. They also studied the effect of the shear on the microdomains of SEBS in clay/SEBS nanocomposites using a small angle neutron scattering. It was found that even though the clay is present, well-aligned HEX of PS block in SEBS/clay nanocomposites toward the flow was epitaxially transformed into twinned BCC when temperature was jumped to BCC.

Even though their work provides a very useful insight on the ODT and OOT transitions in block copolymer-based nanocomposites, the alignment mechanism of block copolymer microdomains as well as the clay layer due to the shear has not been studied in detail. Furthermore, they employed the solution mixing technique, which is not an efficient method to disperse the clay in the block copolymer matrix compared with melt mixing.

Very recently, we investigated in detail the alignment mechanism of HEX and orientational proliferation of HEX after experiencing BCC using an SIS block copolymer with the aid of small angle X-ray scattering (SAXS), rheo-optical device, and transmission electron microscope (TEM) [16]. It is of interest to investigate whether the alignment of HEX and orientational proliferation of HEX are changed when the clay is present. In this study, we study the alignment of HEX of the SIS block copolymer in SIS/clay nanocomposite, using SAXS, rheology, and TEM. Also, the degree of intercalation of the clay in the presence of SIS is investigated with the aid of wide-angle X-ray diffraction (WAXD) and TEM.

2. Experimental

2.1. Materials and sample preparation

Cloisite 20A (Southern Clay Product Inc.) is a montmorillonite modified with dimethyl dihydrogenated tallow ammonium to increase the domain (d) spacing of Na^+-montmorillonite. The cationic exchange capacity (CEC) of Cloisite 20A is 95 meq/100 g. Hereafter, Cloisite 20A is referred to as the clay. The block copolymer employed in this study was a polystyrene-*block*-polyisoprene-*block*-polystyrene (SIS) (V41; Dexco Inc.). The total molecular weight and molecular weight distribution of V41 are 111,000 and 1.07, determined by gel permeation chromatography (Waters Co.) and the calibration curve made by standard PSs. The weight fraction of PS block is 0.18 measured by ^1H nuclear magnetic resonance spectrum (Brucker DRX500). It is noted that V41 has the order to order transition temperature (T_{OOT}) at 175 °C from hexagonally packed cylinders (HEX) to body centered cubic (BCC) microdomains; then a lattice disordering temperature (T_{LDT}) was found at 210 °C [17]. This V41 exhibits very similar behavior of Vector 4111 which was employed in our previous study [16], except lower ($\sim$10 °C) transitions of T_{OOT} and T_{LDT} due to a slightly lower molecular weight (111,000 for V41 versus 118,000 for Vector 4111).

Nanocomposites consisting of V41 with various amounts of the clay were prepared by first dissolving the mixtures in toluene (about 10 wt% of solid) at room temperature for 2 days in the presence of an antioxidant (Irganox 1010, Ciba–Geigy Group), then slowly evaporating the solvent for 2 weeks. After any trace of the solvent was completely removed, the specimens were annealed at 150 °C for 48 h in vacuum. Instead of slow evaporation of toluene, we prepared specimens by the freeze-drying method giving very fast removal of toluene. Other specimens were also prepared by melt mixing of the mixtures at 170 °C by using a Brabender internal mixer with 30 rpm under nitrogen environment, and further annealed at 150 °C for 48 h in vacuum to compare with solution-blended specimens.

The well-aligned HEX cylinders of V41 were prepared by imposing a large amplitude oscillatory shear (LAOS) ($\gamma_0 = 0.99$) and an angular frequency (ω) of 0.8 rad/s at 160 °C using 50 mm diameter parallel plates in a Rheometrics RDS-II with nitrogen purge [16], and the specimens were quenched in ice water. After the alignment, the rectangular bars were cut from three different directions, namely x–y, x–z and y–z planes. The x-, y-, and z-axes correspond to the flow, shear gradient, and vorticity directions, respectively.

2.2. WAXD and SAXS experiment

Wide-angle X-ray diffraction (WAXD) patterns for investigating the d-spacing of the clay were obtained by using a rotating anode X-ray generator (RINT 2000 series; Rigaku) equipped with Pt and Ni double mirrors. The nickel-filtered Cu Kα line ($\lambda = 0.1542$ nm) was utilized as a radiation source. The sample-to-detector distance was 400 mm. In order to investigate the OOT and proliferation of HEX, the SAXS measurements with synchrotron radiations were conducted at the 4C1 beam line at the Pohang Light Source (PLS), Korea [18]. The primary beam was monochromatized with a couple Si(111) single crystal at a wavelength of 0.1598 nm (the photon energy of X-ray is 7.76 keV), and then it was focused on a detector plane by a bent cylindrical mirror. We subtracted the scattering intensity of an empty heating block with two pieces of thin polyimide (Kapton) films from that of samples by taking into account the transmittance of X-rays through the samples. A contribution of the thermal diffuse scattering (TDS) arising from the density fluctuations was further subtracted. We approximated that the intensity at the high q region, where the scattering intensity is independent of q, is identical to the intensity level of TDS. Here, q is the magnitude of the scattering vector, $q = (4\pi/\lambda)\sin(\theta)$, where λ and 2θ are the wavelength of the X-rays and the scattering angle, respectively. The sample thickness was 1 mm and the exposure time was 60 s. A 2-D CCD camera (Princeton

Instruments Inc.; SCX-TE/CCD-1242E) was employed as a detector.

2.3. Transmission electron microscopy

The microdomain structures of the block copolymers were investigated by using a transmission electron microscope (TEM; JEOL 1200EX) operating at 120 kV. Thin film with ~50 nm was obtained by using a microtomer (RMC MT7000) operating at cryogenic condition (−120 °C) and stained with osmium tetroxide (OsO_4) for 15–20 min at room temperature. Due to selective staining, PI matrix appeared black and PS domains white in TEM micrographs.

3. Results and discussion

Fig. 1 gives WAXD spectra of nanocomposites consisting of 3 wt% of the clay and V41 prepared by various methods. It is seen that the d-spacing of the clay in solution is much larger (2.21 nm) than that of the neat clay (compare curve (b) with curve (a)). The large increase in the d-spacing in the solution would be due to the swelling of the surfactant in the clay by solvent; thus large spaces are available to accommodate PS and PI chains into the clay layer. However, during a rapid removal of solvent, many block chains are removed together with solvent from the layer; thus the d-spacing of the clay in specimen (curve (c)) prepared by freeze drying increased very little (~0.2 nm) compared with the clay itself. On the other hand, when solvent was slowly removed at room temperature, the d-spacing (curve (d)) was larger (~0.4 nm) than that of the clay itself. This suggests that the removal of block chains in the clay layer is not severe compared with the freeze-drying specimen. Finally, upon the annealing at 150 °C, the d-spacing of the clay (curve (e)) was increased (~1.0 nm). This is due to the interpenetration of the PS chains into the galley of the clay at temperatures above the glass transition temperature. We noted that the d-spacing of the specimens prepared by melt mixing is essentially the same as that of other specimens prepared by solution casting and annealing, although the WAXD intensity at the peak position for the former specimen is smaller compared with specimen prepared by solution casting and annealing.

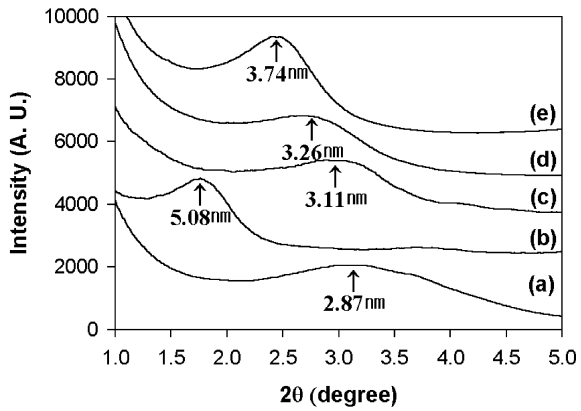

Fig. 1. WAXD intensity versus 2θ for the nanocomposite consisting of V41 and 3 wt% of clay at various preparation stages: (a) clay itself; (b) solution state; (c) after freezing drying; (d) annealing at room temperature for 24 h after slowly removing solvent; (e) annealing at 150 °C for 24 h.

Fig. 2 gives 2-D SAXS patterns as well as TEM micrographs of neat V41 after LAOS. The 2-fold q_m at 0.224 nm^{-1} and $2q_m$ peaks in the q_x–q_y plane in Fig. 2(a) arise from the (100) plane seen in TEM (Fig. 2(A)), and the strong $\sqrt{3}q_m$ peak in the q_x–q_z plane in Fig. 2(b) reflects the (110) plane of HEX shown in Fig. 2(B). Here, q_m represents the scattering vector of the first order SAXS peak. These results imply that the cylinders are well aligned with the (100) plane of the HEX cylinders parallel to the x–z plane. The distinct hexagonal pattern in the z–y plane of Fig. 2(C) is in good agreement with the SAXS result (Fig. 2(c)). The single crystal-like orientations of HEX cylinder by LAOS for V41 are very similar to those for Vector 4111 [16]. In order to quantify the degree of orientation, we evaluate an orientation factor (F_2) in both the xy- and xz-planes [19]:

$$F_2 = C^{-1}[3\langle\cos^2\phi\rangle - 1]/2 \quad (1)$$

$$\langle\cos^2\phi\rangle = \frac{\int_0^{\pi} I(q,\phi)\cos^2\phi\,\sin\phi\,d\phi}{\int_0^{\pi} I(q,\phi)\sin\phi\,d\phi} \quad (2)$$

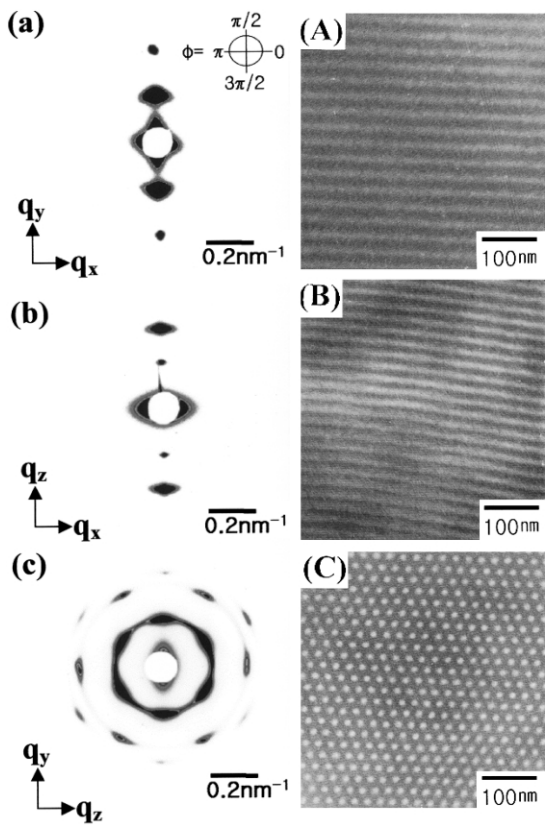

Fig. 2. 2-D SAXS images (a, b, c) and TEM images (A, B, C) for aligned neat V41 at three different planes (x–y, x–z, and z–y).

Here, ϕ is azimuthal angle from the flow direction as indicated in Fig. 2, and C is a conversion constant from the orientation of a cylinder normal to the flow direction [19]:

$$C = [3\langle\cos^2\Phi\rangle - 1]/2 \quad (3)$$

in which Φ is the angle of the cylinder normal to the flow direction and becomes $\pi/2$ (or $3\pi/2$); hence $C = -1/2$. $I(q,\phi)$ was evaluated at $q = q_m$ (0.224 nm^{-1}) in xy-plane for (100) plane and $\sqrt{3}q_m$ peak in xz-plane for (110) plane, respectively. The calculated value of F_2 for both q_x–q_y and q_x–q_z planes was 0.98.

Fig. 3 gives 2-D SAXS and TEM images of three different planes for aligned nanocomposite consisting of V41 and 3 wt% of the clay prepared by melt mixing. We found that the q_m of V41 in the nanocomposite was essentially the same as that of neat V41. It is seen that 2-fold q_m in q_x–q_y plane was clearly seen in Fig. 3(a), and scattering intensity of$\sqrt{3}q_m$ in the q_x–q_z plane is much smaller than that of q_m, as shown in Fig. 3(b).

At lower q regions (between beam stopper and q_m) a large scattering was seen along the y-axis for q_x–q_y and q_z–q_y planes. Interestingly, some extra scatterings at lower q regions are clearly observed at the equatorial plane ($\phi = 0$ and π) in q_x–q_z plane as well as in q_x–q_y plane, whereas

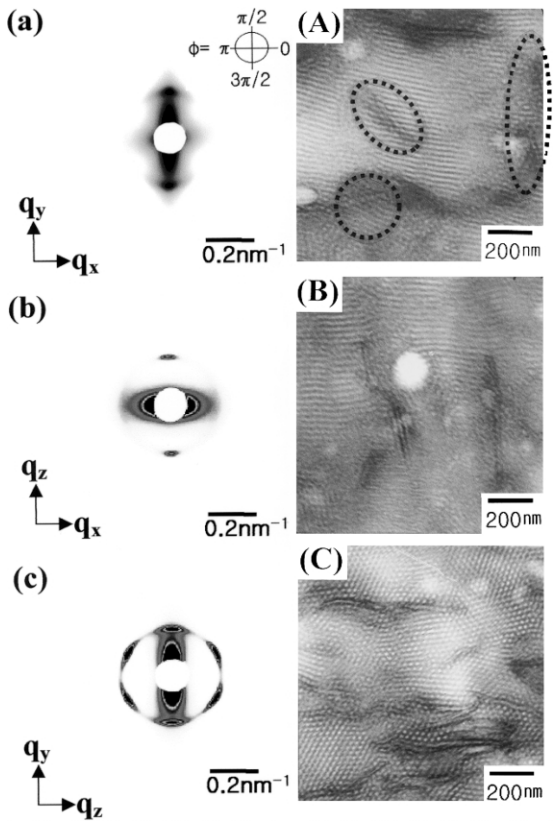

Fig. 3. 2-D SAXS images (a, b, c) and TEM images (A, B, C) for aligned nanocomposite consisting of V41 and 3 wt% of clay at three different planes (x–y, x–z, and z–y). The regions of poor HEX alignment toward the flow direction near tactoids with different orientations are marked by dotted lines in Fig. 3(A).

these are not observed in q_z–q_y plane. We found that for lower q regions (for instance, $q = 0.15$ nm^{-1}), extra scattering intensity level at $\phi = 0$ and π in both q_x–q_z and q_x–q_y planes was 20 times smaller than that at $\phi = \pi/2$ and $3\pi/2$ in either q_x–q_y plane or q_z–q_y plane. The scattering intensity between a beam stopper and q_m was barely seen for neat V41 (see Fig. 2(a)–(c)). Since we used the same beam stopper for all specimens, this intensity was not due to beam stopper; rather the particle scattering of tactoids contributed to extra SAXS scattering at low q regions. Since the particle scattering of tactoids was seen along the y direction as shown in Fig. 3(a) and (c), most tactoids are aligned in x–z plane. This is consistent with TEM images in Fig. 3(A) and (C). However, small amounts of tactoids were aligned in y–z plane, which were observed in Fig. 3(A) and (B). These small portions of tactoids contributed particle scatterings appearing along the x-direction at lower q regions, as shown in Fig. 3(a) and (b).

The values of F_2 calculated at q_m for q_x–q_y plane and $\sqrt{3}q_m$ peak in q_x–q_z plane are 0.64 and 0.42, respectively, which are smaller than those of neat V41. The decreased values of F_2 are due to poor HEX ordering of SIS near tactoids as shown in Fig. 3(A) and (B). Furthermore, the degree of the alignment of tactoids toward the flow direction by LAOS is not so large compared with that of HEX cylinders. We found that the orientation factor F_2 at $q = 1.68$ nm^{-1} corresponding to the clay d-spacing was 0.61 for q_x–q_y plane, which is smaller than that (0.98) at q_m corresponding to the lattice scattering HEX cylinders. Once HEX cylinders are located near some tactoids which are not aligned toward the flow direction, as marked by dotted lines in Fig. 3(A), LAOS cannot align these HEX cylinders toward the flow direction

Fig. 4 gives SAXS images on q_x–q_y and q_x–q_z planes for neat V41 and V41/clay nanocomposite after the specimens are annealed at 190 °C for 10 min. It was found that the T_{OOT} of V41/clay nanocomposites measured by rheology and SAXS was essentially the same (less than 2 °C) as that of neat V41 [17]. Thus, both neat V41 and V41 in nanocomposite have BCC structures at 190 °C. Two sets of q_m at $7\pi/35$ (35°) from shear direction (x-axis) on q_x–q_z plane (Fig. 4(b)) are clearly seen. These peaks come from the $(1\bar{1}0)$ planes of twinned BCC. The distinct appearance of four $\sqrt{2}q_m$ peaks in the q_x–q_z plane in Fig. 4(b) is due to the (200) plane, as noted by Almdal et al. [20] and by Lee et al. [16]. The 2-fold q_m peaks along the q_y axis on q_x–q_y in Fig. 4(a) are from the reflections of (110) plane belonging to each twin. The four weak diagonal peaks of q_m at around $\pi/6$, $5\pi/6$, $7\pi/6$, and $11\pi/6$ on q_x–q_y plane in Fig. 4(a) perhaps result from the overlap of residual intensity of the Gaussian Bragg peaks of the twinned BCC, as described in the previous paper [16]. We found that the 6-fold patterns of q_m and $\sqrt{2}q_m$ were observed in the q_z–q_y plane (the SAXS image was not included here due to the space limit), which indicates again that the cylinders split into BCC along the aligned $\langle 111\rangle$ direction.

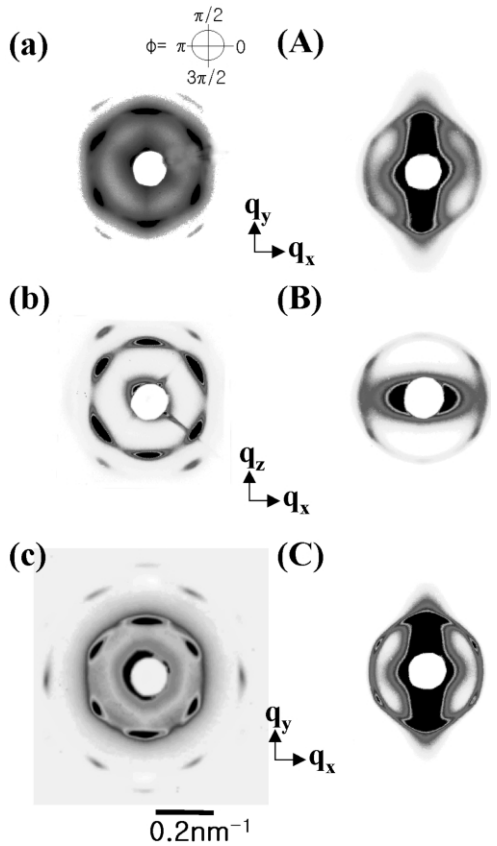

Fig. 4. 2-D SAXS images on q_x-q_y and q_x-q_z planes for neat V41 (a,b) and V41 (A, B) with 3 wt% of clay nanocomposite annealed at 190 °C for 10 min. SAXS images on q_x-q_y plane for neat V41 (c) and V41 (C) with 3 wt% of clay nanocomposite annealed at 160 °C for 1 h after cooling from 190 °C.

The general feature of the formation of twinned BCC at 190 °C for V41/clay nanocomposites is similar to that for neat V41, namely, two sets of q_m at 35° from the shear direction (x-axis) on q_x-q_z plane are seen as shown in Fig. 4(B), even thought these four peaks are weak. The weak peaks are due to the existence of tactoids resulting from a relatively large amount of the clay (3 wt%). Previously, Krishnamoorti and co-workers [14,15] found that these four peaks in $x-z$ plane appeared clearly in small angle neutron scattering images for a nanocomposite with 1 wt% of the clay, and concluded that twinned BCC was formed from HEX cylinders of SEBS in SEBS/caly nanocomposite.

Fig. 4(c) and (C) give 2D SAXS images on q_x-q_y plane for V41 and V41/clay nanocomposites at the first cooling to 160 °C after experiencing BCC at 190 °C. The appearance of $\sqrt{3}q_m$ with the disappearance of $\sqrt{2}q_m$ suggests that the transformation of HEX from twinned BCC was completed at 160 °C for 1 h. The SAXS patterns are completely different from those at 160 °C before heating (compared Fig. 4(c) with Fig. 2(a)). This suggests that during the transition from twinned BCC to HEX some HEX cylinders have different orientations from the shear direction. The angular positions of the q_m become very similar to those at 190 °C irrespective of reflection planes. This indicates that a so-called epitaxial relationship (the spheres along the ⟨111⟩ direction of the BCC lattice have been connected to form the axes of the new HEX phase) was observed from BCC to HEX.

The existence of HEX cylinders with different orientations from original ones (namely, alignment to the flow direction) causes the F_2 value to decrease. The value of F_2 at 160 °C calculated from the q_x-q_y plane was decreased to 0.18 from 0.98 for neat V41, whereas this was 0.38 from 0.68 for V41 in the clay nanocomposite. Interestingly, the decreased value of F_2 for neat V41 is similar to the decreased value of birefrigence data for V4111 which was studied previously [16]. The decreased value of birefringence (or orientation factor) was due to memory effect experienced at twinned BCC state. However, the small decrease of F_2 for V41/nanocomposite compared with neat V41 suggests that the orientation of HEX cylinders near the tactoids (or surface on the clay) does not change even if the specimens are experienced at BCC. This suggests that once all HEX cylinders are located near the tacotids, HEX orientations even after experiencing BCC are not changed much.

4. Conclusion

We have shown that the galley spacing of clay in the SIS/clay nanocomposites measured by WAXD and TEM was increased up to 1.0 nm compared with clay itself, and the nanocomposites clearly showed an intercalated structure. We also found that d-spacing of nanocomposites in solution state was much larger than that of the clay itself. However, this larger space sharply decreased as soon as the solvent was removed fast. The T_{OOT} of V41 in the nanocomposites measured by using synchrotron SAXS and rheology did not change with different amount of clay.

By using 2-D SAXS images and TEM, we have shown that almost all of HEX cylinders in neat SIS are aligned toward the flow direction after the specimens were aligned by a large amplitude of oscillatory shearing. However, some tactoids in nanocomposites are not aligned, although most tactoids are also aligned to the flow direction. Due to HEX cylinders near tactoids, which are not easily aligned toward the flow direction, the orientational factor of HEX cylinders in SIS/clay nanocomposites is smaller than that of neat SIS. Interestingly, once HEX cylinders in SIS/clay nanocomposites are degenerated after experiencing BCC spheres, the decrease in the orientational factor from original well-aligned HEX is smaller compared with neat SIS. This is because PS chains and HEX cylinders tethered on the clay surface did not change with its original alignment.

Acknowledgements

V41 and Cloisite 20A were kindly supplied by DEXCO Inc. and by Southern Clay Co, respectively. This work was supported by National Research Laboratory program governed be MOST, Applied Rheology Center governed by KOSEF. Synchrotron SAXS at the PLS (4C1 and 3C2 beam lines) were supported by MOST and POSCO.

References

[1] Pinnavaia TJ, Beall GW. Polymer–Clay Nanocomposites. New York: Wiley International; 2000. Chap. 1.
[2] Shelley JS, Mather PT, DeVries KL. Polymer 2001;42:5849.
[3] Vaia RA, Jandt KD, Kramer EJ, Giannelis EP. Macromolecules 1995; 28:8080.
[4] Vaia RA, Giannelis EP. Macromolecules 1997;30:7990.
[5] Yoon JT, Jo WH, Lee MS, Ko MB. Polymer 2001;42:329.
[6] Manias E, Chen H, Krishnamoorti R, Genzer J, Kramer EJ, Giannelis EP. Macromolecules 2000;33:7955.
[7] Gilman JW, Jackson CL, Morgan AB, Harris R. Chem Mater 2000;12: 1866.
[8] Okamoto M, Morita S, Kim YH, Kotaka T, Tateyama H. Polymer 2001;42:1201.
[9] Liu X, Wu Q. Polymer 2001;42:10013.
[10] Chen HW, Chang FC. Polymer 2001;42:9763.
[11] Shi H, Lan T, Thomas J, Pinnavaia T. Chem Mater 1996;8:1584.
[12] Kawasumi M, Hasegawa N, Usuki A, Okada A. Appl Clay Sci 1999; 15:93.
[13] Ren J, Silva AS, Krishnamoorti R. Macromolecules 2000;33:3739.
[14] Silva AS, Mitchell CA, Tse MF, Wang H, Krishnamoorti R. J Chem Phys 2001;115:7166.
[15] Krishnamoorti R, Silva AS, Mitchell CA. J Chem Phys 2001;115: 7175.
[16] Lee HH, Jeong WY, Kim JK, K. Ihn J, Kornfield JA, Wang ZG, Qi S. Macromolecules 2002;35:785.
[17] Lee JY. MS Thesis. Korea: Pohang University of Science and Technology; 2002.
[18] Park BJ, Rah SY, Park YJ, Lee KB. Rev Sci Instrum 1995;66:1722.
[19] Sakurai S, Aida S, Okamoto S, Ono T, Imaizumi K, Nomura S. Macromolecules 2001;34:3672.
[20] Almdal K, Koppi KA, Bates FS. Macromolecules 1993;26:40.